Journal of Materials Chemistry A

Accepted Manuscript

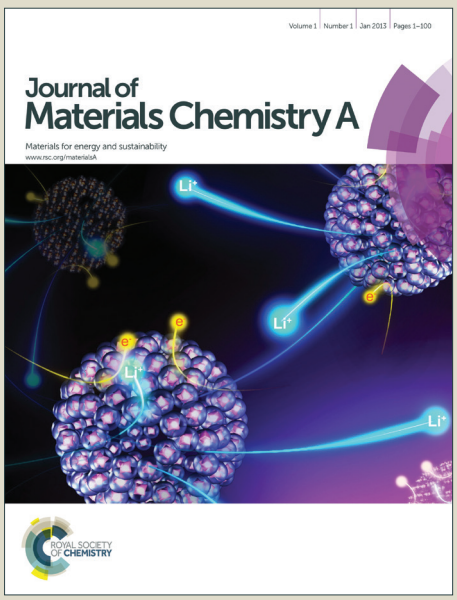

This is an *Accepted Manuscript*, which has been through the Royal Society of Chemistry peer review process and has been accepted for publication.

Accepted Manuscripts are published online shortly after acceptance, before technical editing, formatting and proof reading. Using this free service, authors can make their results available to the community, in citable form, before we publish the edited article. We will replace this *Accepted Manuscript* with the edited and formatted *Advance Article* as soon as it is available.

You can find more information about *Accepted Manuscripts* in the Information for Authors.

Please note that technical editing may introduce minor changes to the text and/or graphics, which may alter content. The journal's standard Terms & Conditions and the Ethical guidelines still apply. In no event shall the Royal Society of Chemistry be held responsible for any errors or omissions in this *Accepted Manuscript* or any consequences arising from the use of any information it contains.

ROYAL SOCIETY OF CHEMISTRY

www.rsc.org/materialsA

Journal Name

RSCPublishing

ARTICLE

Synthesis, Optical, and Photocatalytic Properties of Cobalt Mixed-Metal Spinel Oxides $Co(Al_{1-x}Ga_x)_2O_4$

Kyureon Lee,[a] Daniel A. Ruddy,[b,*] Gordana Dukovic,[a,*] and Nathan R. Neale[b,*]

Cite this: DOI: 10.1039/x0xx00000x

Received ooth January 2012,
Accepted ooth January 2012

DOI: 10.1039/x0xx00000x

www.rsc.org/

Cobalt mixed-metal spinel oxides, $Co(Al_{1-x}Ga_x)_2O_4$, have been predicted to exhibit promising properties as photocatalysts for solar energy conversion. In this work, $Co(Al_{1-x}Ga_x)_2O_4$ were synthesized with a range of $0 \le x \le 1$ via both single-source and multi-source routes. Single-source metal precursors, $[Co\{M(O^tBu)_4\}_2]$ (M= Al or Ga), were decomposed at 300 °C to form amorphous oxides. Multi-source precursors, stoichiometric mixtures of metal acetylacetonate (acac), were used to form nanocrystalline spinel materials. Both were subsequently converted to bulk spinel products by annealing at 1000 °C. The properties of materials fabricated from the single-source and multi-source synthetic routes were compared by analysing data from X-ray diffraction, scanning electron microscopy, transmission electron microscopy, UV-vis spectrophotometry, inductively coupled plasma-optical emission spectroscopy, and gas sorption measurements. The X-ray diffraction data of the materials showed ideal solid solution behavior that followed Vegard's law for both routes, with the multi-source route giving more crystalline bulk material than the single-source route. Absorption data revealed that the absorption onset energies decreased monotonically with increasing x (from 1.84 eV for x = 0 to 1.76 eV for x = 1 from the single-source method; 1.75 eV for x = 0 to 1.70 eV for x = 1 from the multi-source method). The photocatalytic activities of the spinel oxides were evaluated via the photodegradation of methyl orange and phenol, which showed that the photoactivity of $Co(Al_{0.5}Ga_{0.5})_2O_4$ was dependent on both pH and substrate. Remarkably, under appropriate substrate binding conditions (pH 3 with methyl orange), low energy (<2.5 eV) ligand-field transitions contributed between 46–72% of the photoactivity of $Co(Al_{0.5}Ga_{0.5})_2O_4$ prepared from the multi-source route.

1. Introduction

The quest to diversify the world's energy resources from fossil fuels to those derived from renewable and sustainable energy has led to significant researches in both the fundamental and applied sciences.[1-3] Despite great progress, one of the major limitations to widespread adoption of renewable energy is its intermittency – neither the sun nor the wind provides a source of power that continuously matches demands. It is in this context that many researchers are motivated to explore generating fuels directly from sunlight, and in particular hydrogen from solar water splitting.[4-10] The overall water splitting reaction into gaseous hydrogen and oxygen is thermodynamically uphill (ΔG^0 = 238 kJ/mol) and requires efficient catalysts to rapidly shuttle charges away from the photoelectrode surface toward productive proton-coupled electron transfer reactions.[5, 11] For this purpose, semiconductors that function as a monolithic system must be able to satisfy four main requirements: (1) Small band gap energy for absorbing visible light (1.7–2.2 eV), (2) Generation of electrons and holes at the proper potential for reducing protons and oxidizing water, (3) Chemical stability to reducing and oxidizing equivalents in the electrolyte, and (4) Fast transport of photogenerated charge carriers to the semiconductor/electrolyte interface. Metal oxides such as TiO_2 have attracted the attention as a possible candidate due to its photoactivity for water oxidation, low cost, and stability.[4, 5] However, the band gap energy of most metal oxide semiconductors is too large to absorb the visible portion of the solar spectrum, leading to inefficient solar conversion. Finding suitable semiconductors that satisfy all four requirements is a considerable challenge.[5-10]

One intriguing class of candidates that may be able to meet these challenges are cobalt spinel oxides, which have been shown to meet several of the requirements noted above. For

Journal of Materials Chemistry A Accepted Manuscript

example, Woodhouse et al. developed p-type $Co_{3-x-y}Al_xFe_yO_4$ spinel oxides with tuneable band gaps (from 1.6 to 2.0 eV) by varying the Fe/Al ratio. These materials exhibited weak cathodic photocurrent under negative bias.[12, 13] The low PEC response was later attributed to poor electrical conductivity.[14] Related cobalt spinel oxides, CoM_2O_4 (M = Al, Ga, and In), were examined both theoretically and experimentally to understand the optical properties, electronic structure, and PEC performance.[15] This study found that the optical properties are dominated by d → d transitions resulting from Co(II) d orbitals split into Co e_d and t_{2d} states under the tetrahedral crystal field (A site in AB_2O_4 spinel structure).[15] Substituting Ga and In for Al at the B site was found to decrease the band gap through both enhanced O 2p–Ga/In d coupling (driving the valence band edge upward) and increased influence of group 13 cation s states (moving the conduction band downward).[15] In a subsequent study, it was calculated that the electronic structure of these cobalt metal spinel oxides could be further tuned by forming cobalt mixed-metal spinel oxides $Co(Al_xGa_yIn_{1-x-y})_2O_4$ to lower the band gap further and increase orbital mixing, which potentially could lead to enhanced charge carrier mobility.[16]

In this report, we detail efforts to prepare cobalt mixed-metal spinel oxides, $Co(Al_{1-x}Ga_x)_2O_4$, via both single-source and multi-source methods to evaluate the effect of pre-forming Co–O–M bonds on the spinel structural and optical properties. The single-source (ss) molecular precursor method has been explored for synthesizing solid-state materials through both chemical vapor deposition (CVD) and sol-gel techniques.[17-22] This method offers the unique prospect of pre-forming chemical bonds, in this case Co–O–M (M = Al, Ga) in molecular precursors $[Co\{M(O^tBu)_4\}_2]$ (M = Al or Ga) that should be retained in the final material. In contrast, the multi-source (ms) method features individual Co- and M-containing precursors that are decomposed simultaneously and may not exhibit intimate Co and M mixing (which could more easily lead to phase segregation). Non-aqueous synthetic methods for metal spinel oxides nanocrystals (e.g., $CoFe_2O_4$ or $ZnGa_2O_4$) have been reported and were adopted for the multi-source route in the present study.[23-25] The resulting products from each synthetic route were characterized both before and after annealing, and the experimentally obtained optical properties were discussed compared to the predicted ones.[16] Lastly, photocatalytic activity of the materials was tested for the photodegradation of methyl orange.

2. Experimental

All the chemicals were purchased commercially from Sigma-Aldrich unless otherwise noted. Tetrahydrofuran (THF), hexane and tert-butanol (^{t}BuOH) were purified from sodium/benzophenone ketyl, alumina column, and sodium, respectively. $Al(O^tBu)_3$ (technical grade) was purified by dissolving the as-received grey powder (50 g) in hexane (500 mL) and filtering using a cannula filter before recrystallization at -30 °C to yield a colorless powder. The other chemicals employed in the synthesis were used without further purification. All handling and manipulation of air-sensitive compounds were carried out under nitrogen using an inert-atmosphere glove box and/or Schlenk line technique.

2.1 Preparation of $[Ga(O^tBu)_3]_2$

The dimer $[Ga(O^tBu)_3]_2$ was prepared by adding a solution of ^{t}BuOH (4.70 g, 63.4 mmol, 3.1 equiv) in hexanes (60 mL) to a suspension of $[Ga(N(CH_3)_2)_3]_2$ (4.13 g, 20.5 mmol; Strem, 98%) in hexanes (40 mL) and stirring this mixture at room temperature for 15 h. After removing liquid volatiles at room temperature in vacuo, the resulting colorless solid was heated to 50 °C for 1 h to remove the $HN(CH_3)_2$ adduct. This crude product was purified by sublimation at 140 °C (10 mTorr), giving a colorless solid [4.4 g, 75%; ^{1}H NMR (C_6D_6): δ 1.56 (s, 18 H, bridging -O^{t}Bu), δ 1.48 (s, 36 H, terminal -O^{t}Bu)]. This dimer will be referred to as the monomer $Ga(O^tBu)_3$ for simplicity in the Results and Discussion section.

2.2 Synthesis of single-source (ss) molecular precursors, $[Co\{M(O^tBu)_4\}_2]$ (M= Al or Ga)

The single-source molecular precursors were prepared via modification of literature procedures.[26] $CoCl_2$ (130. mg, 1.00 mmol), $Al(O^tBu)_3$ (485 mg, 1.97 mmol) or $[Ga(O^tBu)_3]_2$ (570. mg, 0.985 mmol), and KO^{t}Bu (≥98 %, 221 mg, 1.97 mmol) were loaded into a three neck flask with THF (20 mL) as a solvent. The reaction mixture was heated to reflux for 15 hours under nitrogen atmosphere. The reaction mixture was then cooled to room temperature and the solvent was evaporated under vacuum. The resulting purple solid was extracted with hexanes and filtered via cannula (3 × 10 mL); residual hexanes were removed in vacuo to leave a purple solid (product yield: ~80%).

2.3 Single-source (ss) route to bulk ss-CoM_2O_4 (M= Al or Ga)

A small amount (typically, 150 mg) of the molecular precursor $[Co\{M(O^tBu)_4\}_2]$ (M = Al or Ga), was dissolved in octadecene (ODE, 2 mL) and thermally decomposed under reflux without stirring at 300 °C for 4 h. The as-prepared amorphous oxide CoM_2O_x were collected via filtration (Büchner funnel, in air), and rinsed first with 3 × 5 mL of hexane and then with 3 × 5 mL of ethanol. Amorphous cobalt mixed-metal oxide, $Co(Al_{0.5}Ga_{0.5})_2O_x$, was also prepared through the same procedure using a 1:1 molar ratio of $[Co\{Al(O^tBu)_4\}_2]$ and $[Co\{Ga(O^tBu)_4\}_2]$. The resulting amorphous oxides were heated to 1000 °C with a ramp rate of 20 °C/min and annealed for 1 hour under air to effect crystallization into the spinel phase.

2.4 Multi-source route (ms) to nanoscale ms-CoM_2O_4 (M= Al or Ga) and ms-$Co(Al_{1-x}Ga_x)_2O_4$ (x= 0.25, 0.5, and 0.75) nanocrystals

$Co(acac)_2$ (≥99%, 257.2 mg, 1 mmol), $Al(acac)_3$ (≥99%, 648 mg, 2.00 mmol) or $Ga(acac)_3$ (99.99%, 734 mg, 2.00 mmol), 1,2-tetradecanediol (90%, 1150. mg, 5.00 mmol), oleylamine (70%, 2.82 mL, 6.00 mmol), oleic acid (90 %, 2.21 mL, 6.00 mmol), and benzylether (10 mL) were placed into a

Journal of Materials Chemistry A Accepted Manuscript

 This journal is © The Royal Society of Chemistry 2014

three-neck flask and heated to 40 °C under argon. Upon dissolution of all reagents, the mixture was heated to 100 °C and placed under vacuum (10 mTorr) for 30 min to remove residual O_2 and H_2O. The reaction was heated over 10 min to 200 °C and held for 30 min to nucleate particles, and then heated to refluxed at 280 °C (ramped over 15 min) for 2 h to promote nanocrystal growth; this procedure avoided a wide nanocrystal size distribution that has been reported from direct heating without the nucleation step.[23] The resulting nanocrystals were collected via centrifugation and purified three times by dissolving the products with 5 mL of hexane and by precipitation with a mixture of 2-propanol and ethanol (20 mL each). For the cobalt mixed-metal spinel oxide nanocrystals, $Co(Al_{1-x}Ga_x)_2O_4$ (x = 0.25, 0.5, and 0.75), $Co(acac)_2$ (257 mg, 1.00 mmol), stoichiometric amounts of $Al(acac)_3$ and $Ga(acac)_3$ were used as metal precursors in the above preparation. All the resulting nanocrystals were annealed at 1000 °C for 1 h under air to compare with the bulk ss-$Co(Al_{1-x}Ga_x)_2O_4$.

2.5 Photocatalytic activity test

The photocatalytic activity of $Co(Al_{1-x}Ga_x)_2O_4$ was evaluated via the photodegradation of methyl orange (MO). $Co(Al_{1-x}Ga_x)_2O_4$ (0.02 mmol) materials were dispersed in MO aqueous solution (2 mL, $5x10^{-5}$ M). The pH of these solutions was adjusted by adding HCl for acidic condition or NaOH for basic condition in a quartz cuvette. The reaction sample was sonicated for 2 min and then stirred for 30 min in dark. The sample was then illuminated by a Xe lamp (200 W, Oriel) passing through an AM 1.5G filter. The light intensity was adjusted to 100 mW/cm^2 using a power meter (Newport 407A). To investigate the photocatalytic activity from only visible transition, the AM1.5G light was passed through a 495 nm longpass filter and the light intensity decreased to 66.4 mW/cm^2 (Fig. S5). At hourly intervals, the cuvette was centrifuged to precipitate the suspended particles and achieve an optically transparent MO-containing solution before taking UV-vis absorption spectra.

2.6 Recyclability and stability test of the photocatalysts

To confirm the recyclability and stability of the photocatalyst, recycling ms-$Co(Al_{0.5}Ga_{0.5})_2O_4$ was performed by conducting MO degradation at pH 3 for 6 h, recovering the solid photocatalyst via centrifugation, and adding fresh MO solution. A total of 3 MO solutions were used. The reaction conditions were identical to the above the single experiments, but all quantities were scaled up by a factor of 10 so the recovered oxide catalyst could be examined by XRD before and after the degradation experiments.

2.7 Photodegradation of phenol

Another photodegradation was conducted using a different substrate, phenol, to test the general photocatalytic activity of the photocatlayst. 100 g of solution of phenol in ethanol (200 ppm) was prepared in a pyrex reactor having a quartz window. 100 mg of annealed ms-$Co(Al_{0.5}Ga_{0.5})_2O_4$ was dispersed in the solution via sonication for 2 min, followed by stirring for 30 min in the dark. A solar simulated illumination (AM1.5G, 100 mW) was used as a light source. 1.5 ml of aliquots were withdrawn from the reaction at hourly intervals during 6 hours of the illumination and filtered by a 0.45 µm PTFE syringe filter (MicroLiter Analytical Supplies, Inc.). Phenol concentration of the aliquots was analyzed by GC-MS.

2.8 Characterization

Powder X-ray diffraction (XRD) patterns were collected using Rigaku Ultima IV equipped with Cu K_α radiation (λ = 0.1540562 nm). The crystal domain size was calculated using the Debye-Scherrer equation (L = 0.9 λ / Bcosθ; L: domain size, λ: wavelength of X-ray source, B: full width half maximum). Scanning electron microscopy was carried out using a field emission scanning electron microscope (FESEM, JEOL JSM-7401F) operated at accelerating voltages/working distances of 2.0 kV/1.7 mm and 5.0 kV/9.3 mm for ss- and ms-products, respectively. Transmission electron microscopy (TEM) images were taken using a Philips CM100 microscope operated at accelerating voltage of 80 kV. The absorption spectra of $Co(Al_{1-x}Ga_x)_2O_4$ nanocrystals were recorded by UV–visible absorption spectrophotometer (Agilent 8453). Diffuse reflectance spectra for the bulk $Co(Al_{1-x}Ga_x)_2O_4$ powder samples were collected on a Shimadzu UV-3600 spectrophotometer equipped with an integrating sphere. $BaSO_4$ was used as a reference material. Diffuse reflectance was converted to absorbance using the Kubelka-Munk equation ($A=(1-R_\infty)^2/2R_\infty$; $R_\infty=R_{sample}/R_{reference}$). Elemental analysis was carried out with ARL 3410+ inductively coupled plasma-optical emission spectroscopy (ICP-OES) by the Laboratory for Environmental and Geological Studies (LEGS) at the University of Colorado Boulder. Phenol concentration was determined using an Agilent Technologies 7890A GC system equipped with a flame-ionization detector (FID) and an Agilent Technologies 5975C inert XL mass selective detector (MSD). An Agilent 19091S-433 HP-5MS capillary GC column was used (30 m x 0.250 mm I.D. X0.25 mm film thickness 5% phenyl-95% methylsiloxane).

3. Results and Discussion

3.1 Single-source (ss) route to bulk spinel oxides, ss-$Co(Al_{1-x}Ga_x)_2O_4$ (x= 0, 0.5, and 1)

$$CoCl_2 + 2\ M(O^tBu)_3 + 2\ KO^tBu \xrightarrow[\text{reflux in THF}]{\text{-2 KCl}} [Co\{M(O^tBu)_4\}_2]$$
(M= Al or Ga)

$$[Co\{M(O^tBu)_4\}_2] \xrightarrow[\text{ODE, 300 °C}]{} \text{Amor. } CoM_2O_x \xrightarrow[\text{1000 °C}]{} CoM_2O_4$$

$$[Co\{Al(O^tBu)_4\}_2] + [Co\{Ga(O^tBu)_4\}_2] \xrightarrow[\text{ODE, 300 °C}]{} \text{Amor. } Co(Al_{1-x}Ga_x)_2O_x \xrightarrow[\text{1000 °C}]{} Co(Al_{1-x}Ga_x)_2O_4$$

Scheme 1. Single-source route to bulk ss-$Co(Al_{1-x}Ga_x)_2O_4$.

Journal of Materials Chemistry A Accepted Manuscript

Single-source molecular precursors $[Co\{M(O^tBu)_4\}_2]$ (M = Al or Ga) were synthesized by the reaction of $CoCl_2$ with $M(O^tBu)_3$ and KO^tBu. These complexes were then thermally decomposed to form bulk ss-$Co(Al_{1-x}Ga_x)_2O_4$ as shown in Scheme 1. A similar process was reported by Meyer et al. for nanoscale $CoAl_2O_4$ spinel oxides, but in that case the $[Co\{Al(O^tBu)_4\}_2]$ precursor decomposition was accomplished via hydrolysis within a micro-emulsion.[17] Here, the single-source molecular precursors $[Co\{Al(O^tBu)_4\}_2]$ and $[Co\{Ga(O^tBu)_4\}_2]$ were thermally decomposed in anhydrous solvent (octadecene, ODE) at 300 °C, which should result in better retention of the Co–O–M structural motif (which can decompose under hydrolysis conditions) in the amorphous $CoAl_2O_x$ and $CoGa_2O_x$ products. Several routes to the ss molecular precursor $[Co\{Al_{0.5}Ga_{0.5}(O^tBu)_4\}_2]$ were unsuccessful. For instance, reaction of 1:1:1 molar ratio $CoCl_2$, $Al(O^tBu)_3$, and $Ga(O^tBu)_3$ conducted identically to that above provided a purple powder that contained a 1:1.17:0.86 ratio of Co/Al/Ga that is close to the expected values. Both FTIR and UV-vis absorbance data showed features resembling those of the di-substituted complexes $[Co\{Al(O^tBu)_4\}_2]$ and $[Co\{Ga(O^tBu)_4\}_2]$ that suggested the presence of Co–O, Al–O, and Ga–O structural units (Fig. S1), but given the metal ratio did not appear to be tuneable based on the initial stoichiometry (likely owing to different reactivity rates of the $Al(O^tBu)_3$ and $Ga(O^tBu)_3$ precursors), this strategy was not pursued further. Similarly, reaction of a 1:1 molar ratio of $CoCl_2$ and $Al(O^tBu)_3$ did not give the desired mono-substituted product $ClCoAl(O^tBu)_4$ but instead yielded the purple di-substituted $[Co\{Al(O^tBu)_4\}_2]$. Thus, the amorphous cobalt mixed metal oxide, $Co(Al_{0.5}Ga_{0.5})_2O_x$, was prepared by decomposition of a 1:1 molar ratio of $[Co\{Al(O^tBu)_4\}_2]$ and $[Co\{Ga(^tOBu)_4\}_2]$.

As shown in Fig. 1, as-prepared $CoAl_2O_x$ and $CoGa_2O_x$ exhibit X-ray diffraction patterns consistent with an amorphous structure. In-situ annealing experiments from 500 to 1000 °C showed that conversion from amorphous to the spinel structure

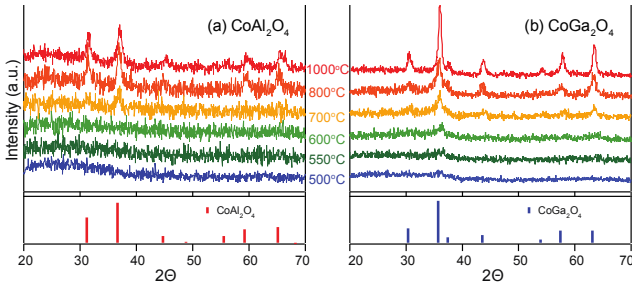

Figure 1. Powder X-ray diffraction patterns of the products obtained from annealing the amorphous (a) $CoAl_2O_x$ and (b) $CoGa_2O_x$ at varying temperature (500 – 1000 °C). The amorphous oxides (CoM_2O_x) were crystallized to spinel oxides (CoM_2O_4) with increasing annealing temperature. The vertical lines below the X-ray diffraction patterns represent the expected peak positions of spinel oxides (PDF#00-010-0458 for $CoAl_2O_4$; PDF#00-011-0698 for $CoGa_2O_4$).

began near 700 °C for $CoAl_2O_4$ and 550 °C for $CoGa_2O_4$ (as evidenced by a peak for the (311) reflection at 36.8° for $CoAl_2O_4$ and at 35.7° for $CoGa_2O_4$), but more highly crystalline material with sharper peaks required temperatures of 1000 °C. Interestingly, crystallization occurred at lower temperatures for $CoAl_2O_x$ prepared from $[Co\{Al(O^tBu)_4\}_2]$ under anhydrous conditions than that from hydrolysis in micelles, which required 800 °C before the spinel phase was observed.[17] This result suggests that decomposition of ss molecular precursors under anhydrous conditions preserves better the Co–O–Al structural unit that then leads to a lower barrier to crystallization.

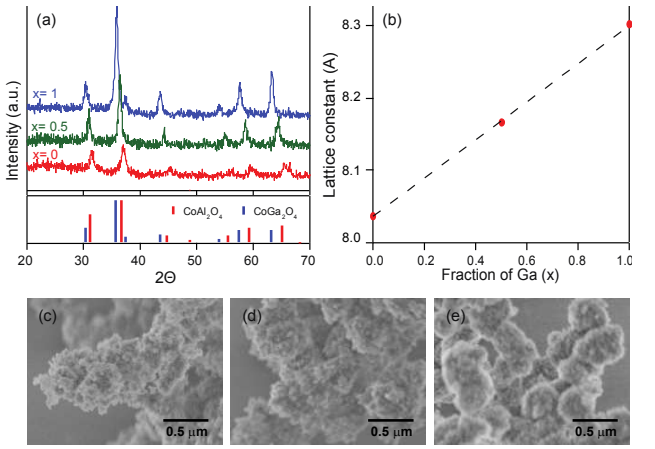

Figure 2. (a) Powder X-ray diffraction patterns of ss-$Co(Al_{1-x}Ga_x)_2O_4$ annealed at 1000 °C. The vertical lines below the X-ray diffraction patterns represent the expected peak positions of spinel oxides (PDF#00-010-0458 for $CoAl_2O_4$; PDF#00-011-0698 for $CoGa_2O_4$). (b) lattice parameter plotted against the fraction of Ga (x). Scanning electron micrographs of ss-$Co(Al_{1-x}Ga_x)_2O_4$, x= 0 (c), x = 0.5 (d), and x= 1 (e).

XRD patterns of ss-$Co(Al_{1-x}Ga_x)_2O_4$ (x = 0, 0.5, and 1) prepared by annealing the amorphous $Co(Al_{1-x}Ga_x)_2O_x$ under air at 1000 °C for 1 h are shown in Fig. 2(a). The diffraction peaks of $CoGa_2O_4$ appear at lower angles with respect to those of $CoAl_2O_4$ as the ionic radius of Ga is larger than Al. Interestingly, the diffraction peaks of $Co(Al_{0.5}Ga_{0.5})_2O_4$ show single patterns of spinel structure and were located between the diffraction peaks of $CoAl_2O_4$ and $CoGa_2O_4$. The lattice parameter, *a*, calculated from the (311) reflection, is plotted as a function of Ga fraction (x) in Fig. 2(b). Lattice parameter *a* increases linearly demonstrating ideal solid solution behavior according to Vegard's law. ICP-OES elemental analysis showed the ratios between the metals in the $Co(Al_{0.5}Ga_{0.5})_2O_4$ did not significantly change from the initial ratios of metal precursors (see Table S1). These observations from XRD and elemental analyses indicate that a solid solution of $CoAl_2O_4$ and $CoGa_2O_4$ was successfully synthesized through this synthetic route without phase segregation and also imply other product compositions could be synthesized by varying the molar ratio of $[Co\{Al(O^tBu)_4\}_2]$ and $[Co\{Ga(^tOBu)_4\}_2]$ precursors. Scanning electron micrographs of the ss-$Co(Al_{1-x}Ga_x)_2O_4$ samples annealed to 1000 °C display micron-sized agglomerates composed of irregular shaped nanoscale particles for all three compositions. The nanoscale, polycrystalline nature of this material is consistent with the small domain size (~15 nm) calculated using the Scherrer equation applied to the XRD data (Fig. 2(a)).

Journal of Materials Chemistry A Accepted Manuscript

This journal is © The Royal Society of Chemistry 2014

3.2 Multi-source (ms) route to nano and bulk spinel oxides, ms-$Co(Al_{1-x}Ga_x)_2O_4$ (x= 0, 0.25, 0.50, 0.75, and 1)

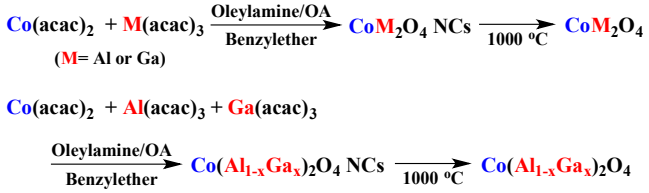

Scheme 2. Multi-source (ms) route to nano ss- $Co(Al_{1-x}Ga_x)_2O_4$ and bulk annealed ss-$Co(Al_{1-x}Ga_x)_2O_4$.

Nonaqueous solution phase reactions have been shown to give nanocrystalline spinel oxide material without annealing and were adopted to prepare samples via the ms route in this study.[23-25] Scheme 2 shows the preparation of ms-$Co(Al_{1-x}Ga_x)_2O_4$ (x= 0, 0.25, 0.50, 0.75, and 1) nanocrystals from cobalt and Al or Ga acac precursors. Briefly, $Co(acac)_2$ was combined with a stoichiometric amount of $Al(acac)_3$ and/or $Ga(acac)_3$ in the presence of oleylamine, oleic acid, and 1,2-hexadecanediol in benzylether, and this mixture was heated to high temperature (280 °C), leading to hexane-soluble $Co(Al_{1-x}Ga_x)_2O_4$ nanocrystals. The x values of the products were determined by ICP-OES elemental analysis (see Table S1). The ratios between the metals of the resulting nanocrystals were similar to the ratios of metal precursors that were used in the reaction, suggesting that the ms-$Co(Al_{1-x}Ga_x)_2O_4$ materials also exhibit homogeneous incorporation of both Al and Ga.

In contrast to the amorphous oxides obtained from the decomposition of ss precursors, XRD patterns of as-prepared ms-$Co(Al_{1-x}Ga_x)_2O_4$ exhibit diffraction peaks that can be indexed to cubic spinel patterns without any post-synthesis annealing (Fig. 3(a)). The average grain size of the nanocrystals calculated by a Debye-Scherrer equation is ~5 nm (Fig. 3(d)).

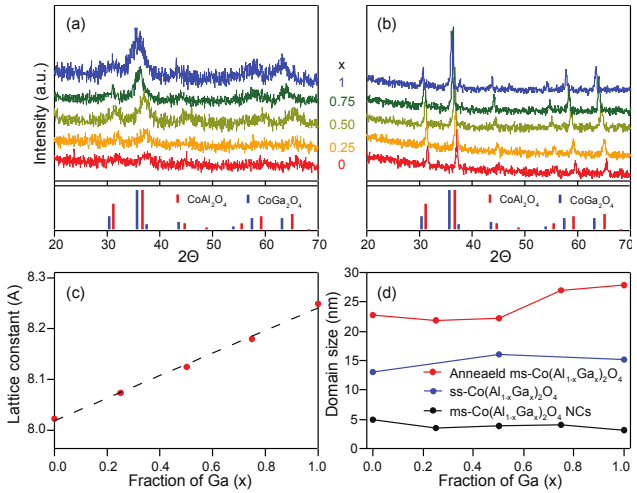

Figure 3. Powder X-ray diffraction patterns of (a) ms-$Co(Al_{1-x}Ga_x)_2O_4$ nanocrystals and (b) annealed ms-$Co(Al_{1-x}Ga_x)_2O_4$ at 1000 °C for 1 hour. The vertical lines below the X-ray diffraction patterns represent the expected peak positions of spinel oxides (PDF#00-010-0458 for $CoAl_2O_4$; PDF#00-011-0698 for $CoGa_2O_4$). (c) Lattice parameters, *a*, determined by the (311) reflection against Ga content (x). (d) Domain size of ms-$Co(Al_{1-x}Ga_x)_2O_4$ nanocrystals, annealed (1000 °C, 1h) ss- and ms- $Co(Al_{1-x}Ga_x)_2O_4$ calculated using Debye-Scherrer equation.

The nanocrystals were subsequently annealed at 1000 °C for 1 hour in order to increase the grain size and compare directly with the spinel products obtained from the single-source route. The XRD patterns of the annealed ms-$Co(Al_{1-x}Ga_x)_2O_4$ are shown in Fig. 3(b). Similar to the spinel materials from the ss method, the peaks of ms-$CoGa_2O_4$ appear at lower diffraction angles than ms-$CoAl_2O_4$. The solid solutions, ms-$Co(Al_{1-x}Ga_x)_2O_4$, showed linear correlation between the lattice parameters and compositions (x), satisfying Vegard's law (Fig. 3(c)). The domain size of the annealed nanoparticles is ~25 nm which is larger than that of the products from the ss route (cf. ~15 nm), indicating the ms route leads to larger grain size products under the same annealing conditions. This result could be rationalized that the initial ~5 nm crystallites from the ms route require less thermal energy for the larger grain growth than that required for the single-source route.

The low resolution transmission electron micrographs of the as-prepared ms-$Co(Al_{1-x}Ga_x)_2O_4$ nanocrystals show a mixture of shapes and no large agglomerates (Figs. 4(a–c)) consistent with the ~5 nm crystallite size of the $Co(Al_{1-x}Ga_x)_2O_4$ nanocrystals calculated from the XRD patterns. Scanning electron micrograph (SEM) images of annealed ms-$Co(Al_{1-x}Ga_x)_2O_4$ at 1000 °C are shown in Figs. 4(d–f), and all the compositions exhibit faceted particles on the micrometer scale. The nanocrystals appear to serve as seeds for grain growth to ~25 nm (from XRD analysis). Consistent with this observation, large, non-porous monoliths result from annealing nanocrystalline ms-$Co(Al_{1-x}Ga_x)_2O_4$ to high temperatures that contrasts the more porous structure resulting from annealing amorphous ss-$Co(Al_{1-x}Ga_x)_2O_x$ (Fig. 2c-e). BET surface area measurements also indicate the ss method gave a material with a slightly higher surface area (10.1 m^2/g) than that from the ms method (8.1 m^2/g; see Table S2). The larger grain size and monolithic structure of annealed ms-$Co(Al_{1-x}Ga_x)_2O_4$ may be more suitable for photoelectrochemical applications since it may lead to improved charge transport to the photocatalyst surface when compared to ss-$Co(Al_{1-x}Ga_x)_2O_4$ annealed at the same temperature.

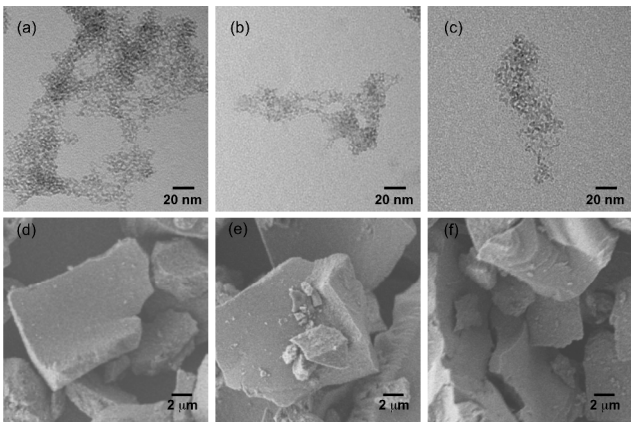

Figure 4. Transmission electron micrographs of the ms-$Co(Al_{1-x}Ga_x)_2O_4$ nanoparticles, x = 0 (a), x= 0.5 (b), and x= 1 (c). Scanning electron micrographs of the annealed ms-$Co(Al_{1-x}Ga_x)_2O_4$, x = 0 (d), x= 0.5 (e), and x= 1 (f).

Journal of Materials Chemistry A Accepted Manuscript

3.3 Optical properties of $Co(Al_{1-x}Ga_x)_2O_4$ materials

Diffuse reflectance spectra were obtained from ss-$Co(Al_{1-x}Ga_x)_2O_4$ and ms-$Co(Al_{1-x}Ga_x)_2O_4$ bulk powders, shown in Fig. 5 (a) and (b). The samples from both synthetic routes were annealed at 1000 °C for 1 h. Transmittance mode UV-vis absorbance spectra from hexane solutions of ms-$Co(Al_{1-x}Ga_x)_2O_4$ nanocrystals are shown in Fig. S2 for comparison. For all samples, low energy absorbance features from 1.7 to 2.4 eV result from tetrahedral Co^{2+} $^4A_2 \rightarrow {}^4T_1(P)$ ligand-field transitions,[27] which have been observed for both bulk[28] and nanoscale[29, 30] Co^{2+}:ZnO. These absorbance features confirm the presence of Co^{2+} in the tetrahedral spinel A site. The absorption onsets shift from 1.84 eV for x = 0 to 1.76 eV for x = 1 (for ss-$Co(Al_{1-x}Ga_x)_2O_4$) and from 1.75 for x = 0 to 1.70 eV for x = 1 (for ms-$Co(Al_{1-x}Ga_x)_2O_4$); Fig. 5(c)). The shift to lower energy transitions with increasing Ga content for both ss- and ms-$Co(Al_{1-x}Ga_x)_2O_4$ is consistent with the prediction that the increasing lattice parameters owing to the larger Ga atom (cf. Al) reduces the crystal field splitting of Co^{2+} d states.[16] However, it is found that these $^4A_2 \rightarrow {}^4T_1(P)$ ligand-field transitions also dominate the lower energy optical absorption even for complete Ga substitution (x = 1). This contrasts the prediction that the Ga 4s states should become lower in energy than that of the Co d states (and lead to a Co d → Ga s transition) for Ga values of $x \geq 0.75$.[16] This result suggests a possible band structure where the metal s states are located at higher energy state than Co d orbital (t_{2d}) for all values of x as shown in Fig. 5(d). Alternatively, lower energy absorption for Ga-rich compositions may have some contribution from other transitions such as defect-mediated field transitions resulting from these preparation methods.

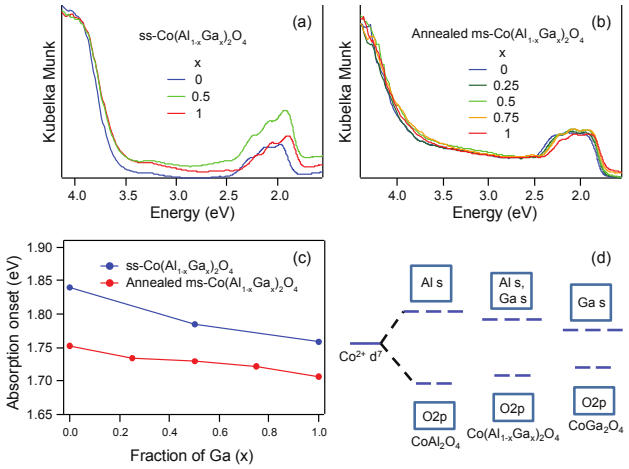

Figure 5. Diffuse reflectance spectra of annealed (1000 °C, 1 h): (a) ss-$Co(Al_{1-x}Ga_x)_2O_4$; (b) ms-$Co(Al_{1-x}Ga_x)_2O_4$ with varying x; (c) absorption onsets as a function of x; (d) suggested band structure of $Co(Al_{1-x}Ga_x)_2O_4$.

3.4 Photocatalytic degradation of methyl orange (MO)

Photocatalytic degradation of methyl orange (MO) dye under simulated solar illumination was investigated to evaluate the possibility of performing productive redox chemistry with photogenerated charges from the cobalt mixed-metal oxide spinels. Though it was not studied in detail here, the MO degradation mechanism catalyzed by the metal oxides TiO_2[31] and ZnO[32] are known to proceed via both oxidative and reductive pathways. The comparison of activities between ss- and ms-$Co(Al_{1-x}Ga_x)_2O_4$ photocatalysts at pH 3 is shown in Fig. 6(a). After 6 hours of simulated solar illumination, MO degradation was enhanced in the presence of annealed ss- or ms-$Co(Al_{0.5}Ga_{0.5})_2O_4$ relative to control experiments illuminating MO solutions with no oxide added. Despite the 25% higher surface area of ss-$Co(Al_{1-x}Ga_x)_2O_4$, the ms-$Co(Al_{1-x}Ga_x)_2O_4$ had higher activity for MO degradation, which could be due to the larger grain size for the annealed ms-$Co(Al_{0.5}Ga_{0.5})_2O_4$ as noted above. Additionally, dark adsorption measurements at pH 3 showed that ms-$Co(Al_{1-x}Ga_x)_2O_4$ adsorbed 10% more molecules of MO per unit area (0.43 molecules/nm^2) than ss-$Co(Al_{1-x}Ga_x)_2O_4$ (0.39 molecules/nm^2) as shown in Fig. S3 and Table S2, which could also account for the higher photocatalytic activity of ms-$Co(Al_{1-x}Ga_x)_2O_4$.

The degree of MO adsorption is highly dependent on the pH, with MO adsorption decreasing by an order of magnitude upon increasing the pH from 3 to 9 for ms-$Co(Al_{0.5}Ga_{0.5})_2O_4$ (Fig. S4 and summarized in Fig. 6(b)). Unsurprisingly from this result, the degree of photocatalytic MO degradation was strongly pH dependent, with a 3-fold increase in MO degradation at pH 3 versus at pH 9 (Fig. 6(b)). The pH dependence may be explained by surface charging of the catalyst given that the points of zero charge (PZC)[31, 33] for Al_2O_3[34], Ga_2O_3[35], and Co_2O_3[36] are all greater than pH 7. Under acidic conditions at pH values less than the PZC, we hypothesize that the surface of the spinel is protonated and more readily adsorbs the dye via the MO sulfate group, promoting degradation. Conversely, at higher pH values than

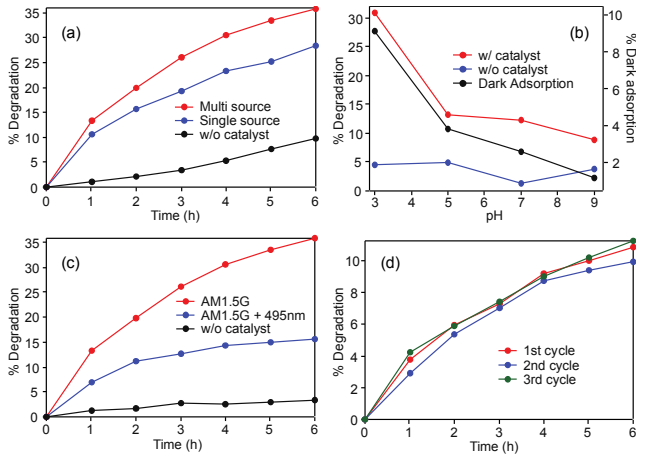

Figure 6. (a) Photodegradations of MO with annealed ms- or ss-$Co(Al_{0.5}Ga_{0.5})_2O_4$ at pH 3 over 6 h illumination. (b) pH effect on photodegradation of MO with (red) and without (blue) annealed ms-$Co(Al_{0.5}Ga_{0.5})_2O_4$) under 4 h of illumination. Black points correspond to the dark adsorption of MO molecules to the photocatalyst surface. (c) Photodegradation of MO with annealed ms-$Co(Al_{0.5}Ga_{0.5})_2O_4$ at pH 3 under full spectrum solar simulated illumination (red, w/ AM1.5G filter) and visible light irradiation (blue) using a AM1.5G filter and a 495 nm long pass filter. (d) Recycling experiment showing the photodegradation rate of MO at pH 3 under visible illumination is retained when using the same annealed ms-$Co(Al_{0.5}Ga_{0.5})_2O_4$ sample for 3 fresh MO solutions.

Journal of Materials Chemistry A Accepted Manuscript

This journal is © The Royal Society of Chemistry 2014

the PZC, the negatively charged spinel oxide surface repels the anionic MO sulfate group, reducing the dye adsorption and thus slowing degradation.

In Fig. 6(c), the MO degradation was probed using both AM1.5G filter and 495 nm longpass filter (blue), which only transmits light <2.5 eV that would be absorbed only by the Co^{2+} $^4A_2 \rightarrow {}^4T_1(P)$ ligand-field transitions. Remarkably, 46% of the total degradation relative to full spectrum light from the simulated solar illumination was observed (35% degradation after 6 h under full spectrum; cf. 16% under visible light). Moreover, this observation agrees with the apparent quantum efficiency,[37] which does not take into account light absorbed but only light impinging upon the sample. The apparent quantum efficiency was 2.4×10^{-4}% for initial MO degradation (0–1 h) under visible illumination, which is 72% of the 3.4×10^{-4}% apparent quantum efficiency observed for full spectrum illumination (Table S3). Importantly, these results demonstrate that the redox equivalents photogenerated by these lower energy transitions contribute significantly (between 46–72%) to catalytic MO degradation.

To assess the stability of the photocatalyst, three successive MO degradation experiments were carried out by recycling the used annealed ms-$Co(Al_{0.5}Ga_{0.5})_2O_4$ and adding this to a fresh MO solution. As shown in Fig. 6(d), the photocatalytic activity was retained, and the photocatalyst did not change appreciably after the recycling as evidenced by XRD (Fig. S6).

Finally, Bae et al. have demonstrated that a single photocatalytic activity test does not represent the general activity of a photocatalyst.[38] To explore the general photocatalytic activity of these cobalt spinel oxides, we conducted similar degradation tests using phenol as a substrate instead of MO. After illuminating a 200 ppm solution of phenol in ethanol for 6 h under full spectrum in the presence of annealed ms-$Co(Al_{0.5}Ga_{0.5})_2O_4$, no phenol degradation was observed by GC-MS. Though an exhaustive effort to explore a variety of reaction conditions and substrates was not conducted, these preliminary experiments suggest that the photocatalytic degradation provided by these cobalt spinel oxides is substrate-specific. However, although we do not have evidence of generalized photocatalytic activity, the observed visible response for MO degradation, with 46–72% of the degradation coming from the visible part of the solar spectrum, demonstrates that the transitions in the visible part of the spectrum of these spinel materials can be photoactive.

4. Conclusions

In summary, we have developed single-source and multi-source synthetic routes for $Co(Al_{1-x}Ga_x)_2O_4$. Whereas spinel oxide materials from single-source precursors required annealing to induce crystallization, the multi-source route produced nanoscale spinel products without annealing. Annealing amorphous materials from the single-source route to 1000 °C gave ~15 nm crystallites, and identical heat treatment on the nanocrystalline material from the multi-source method grew the grain size from ~5 nm to ~25 nm. Both methods afforded ideal solid solutions of the mixed Al-Ga compounds. The optical properties of $Co(Al_{1-x}Ga_x)_2O_4$ were found to be consistent with $^4A_2 \rightarrow {}^4T_1(P)$ ligand-field transitions dominating the lower energy optical properties for all compositions. Finally, the photocatalytic activities of $Co(Al_{1-x}Ga_x)_2O_4$ materials from both routes showed that, despite a higher surface area for materials from the single-source route, spinel oxides from the multi-source method adsorbed more methyl orange substrate per unit surface area. The degree of substrate adsorption was critical to the photocatalytic activity, which was found to be highly dependent on the substrate surface affinity. Remarkably, under appropriate substrate binding conditions, photogenerated redox equivalents from low energy (1.7–2.5 eV) ligand-field transitions contribute 46–72% to the photocatalytic activity of these cobalt spinel oxides.

Acknowledgements

Molecular and material synthesis and characterization was funded by NREL's Laboratory Directed Research and Development (LDRD) program. Photocatalytic experimental design and data interpretation was supported by the U.S. Department of Energy, Office of Science, Office of Basic Energy Sciences, Division of Chemical Sciences, Geosciences, and Biosciences through Contract No. DE-AC36-08GO28308 to NREL.

Notes and references

[a] Department of Chemistry and Biochemistry, University of Colorado Boulder, Boulder, CO 80309.
[b] Chemistry and Nanoscience Center, National Renewable Energy Laboratory, Golden, CO 80401.

† Electronic Supplementary Information (ESI) available: Elemental analysis results obtained by ICP-OES; UV-vis absorbance and DRIFTS spectra of molecular precursor complexes; and UV-vis absorbance spectra of ms-$Co(Al_{1-x}Ga_x)O4$ nanocrystals. See DOI: 10.1039/b000000x/

1. J. A. Turner, *Science*, 1999, **285**, 687-689.
2. N. S. Lewis, *MRS Bulletin*, 2007, **32**, 808-820.
3. M. Z. Jacobson, W. G. Colella and D. M. Golden, *Science*, 2005, **308**, 1901-1905.
4. A. Fujishima and K. Honda, *Nature*, 1972, **238**, 37-38.
5. M. D. Hernández-Alonso, F. Fresno, S. Suárez and J. M. Coronado, *Energy Environ. Sci.*, 2009, **2**, 1231-1257.
6. O. Khaselev and J. A. Turner, *Science*, 1998, **280**, 425-427.
7. A. Kudo and Y. Miseki, *Chem. Soc. Rev.*, 2008, **38**, 253-278.
8. B. D. Alexander, P. J. Kulesza, I. Rutkowska, R. Solarska and J. Augustynski, *J. Mater. Chem.*, 2008, **18**, 2298-2303.
9. J. E. Yourey and B. M. Bartlett, *J. Mater. Chem.*, 2011, **21**, 7651-7660.
10. Y. Park, K. J. McDonald and K.-S. Choi, *Chem. Soc. Rev.*, 2013, **42**, 2321-2337.
11. J. E. Funk and R. M. Reinstrom, *Ind. Eng. Chem. Proc. Des. Dev.*, 1966, **5**, 336-342.
12. M. Woodhouse, G. S. Herman and B. A. Parkinson, *Chem. Mater.*, 2005, **17**, 4318-4324.
13. M. Woodhouse and B. A. Parkinson, *Chem. Mater.*, 2008, **20**, 2495-2502.
14. A. Walsh, S.-H. Wei, Y. Yan, M. M. Al-Jassim, J. A. Turner, M. Woodhouse and B. A. Parkinson, *Phys. Rev. B*, 2007, **76**, 165119.

Journal of Materials Chemistry A Accepted Manuscript

15. A. Walsh, K.-S. Ahn, S. Shet, M. N. Huda, T. G. Deutsch, H. Wang, J. A. Turner, S.-H. Wei, Y. Yan and M. M. Al-Jassim, *Energy Environ. Sci.*, 2009, **2**, 774-782.
16. C. Feng, W.-J. Yin, J. Nie, X. Zu, M. N. Huda, S.-H. Wei, M. M. Al-Jassim, J. A. Turner and Y. Yan, *Appl. Phys. Lett.*, 2012, **100**, 023901.
17. F. Meyer, R. Hempelmann, S. Mathur and M. Veith, *J. Mater. Chem.*, 1999, **9**, 1755-1763.
18. M. Veith, *J. Chem. Soc., Dalton Trans.*, 2002, 2405-2412.
19. M. Veith, M. Haas and V. Huch, *Chem. Mater.*, 2005, **17**, 95-101.
20. N. Tomar, E. Ghanti, A. K. Bhagi and R. Nagarajan, *J. Non-Cryst. Solids*, 2009, **355**, 2657-2662.
21. E. Ghanti and R. Nagarajan, *Dalton Trans.*, 2010, **39**, 6056-6061.
22. K. Fujdala, R. Brutchey and T. D. Tilley, in *Surface and Interfacial Organometallic Chemistry and Catalysis*, eds. C. Copéret and B. Chaudret, Springer Berlin Heidelberg, 2005, vol. 16, pp. 69-115.
23. S. Sun, H. Zeng, D. B. Robinson, S. Raoux, P. M. Rice, S. X. Wang and G. Li, *J. Am. Chem. Soc.*, 2004, **126**, 273-279.
24. H.-J. Byun, J.-U. Kim and H. Yang, *Nanotechnology*, 2009, **20**, 495602.
25. J. Lee, S. Zhang and S. Sun, *Chem. Mater.*, 2013, **25**, 1293-1304.
26. G. Garg, R. K. Dubey, A. Singh and R. C. Mehrotra, *Polyhedron*, 1991, **10**, 1733-1739.
27. F. A. Cotton, D. M. L. Goodgame and M. Goodgame, *J. Am. Chem. Soc.*, 1961, **83**, 4690-4699.
28. H. A. Weakliem, *J. Chem. Phys.*, 1962, **36**, 2117-2140.
29. P. V. Radovanovic, N. S. Norberg, K. E. McNally and D. R. Gamelin, *J. Am. Chem. Soc.*, 2002, **124**, 15192-15193.
30. D. A. Schwartz, N. S. Norberg, Q. P. Nguyen, J. M. Parker and D. R. Gamelin, *J. Am. Chem. Soc.*, 2003, **125**, 13205-13218.
31. Y. R. Smith, A. Kar and V. Subramanian, *Ind. Eng. Chem. Res.*, 2009, **48**, 10268-10276.
32. J. R. Darwent and A. Lepre, *J. Chem. Soc., Faraday Trans. 2*, 1986, **82**, 1457-1468.
33. W. Zhang, J. Zhang, X. Lan, Z. Chen and T. Wang, *Catal. Commun.*, 2010, **11**, 1104-1108.
34. M. Kosmulski, *J. Colloid Interface Sci.*, 2002, **253**, 77-87.
35. M. Kosmulski, *J. Colloid Interface Sci.*, 2001, **238**, 225-227.
36. P. H. Tewari and A. B. Campbell, *J. Colloid Interface Sci.*, 1976, **55**, 531-539.
37. J. M. Buriak, P. V. Kamat and K. S. Schanze, *ACS Applied Materials & Interfaces*, 2014, **6**, 11815-11816.
38. S. Bae, S. Kim, S. Lee and W. Choi, *Catal. Today*, 2014, **224**, 21-28.

Journal of Materials Chemistry A Accepted Manuscript

This journal is © The Royal Society of Chemistry 2014